IEEE Open Journal of
Industry Applications

Received 11 November 2025; revised 2 February 2026; accepted 13 February 2026. Date of publication 16 February 2026; date of current version 3 March 2026.

Digital Object Identifier 10.1109/OJIA.2026.3665327

Ferrite Plate Multiobjective Topology Optimization in a Wireless Power Transfer System for UAV Charging

GIULIO POGGIANA [1,2], MOHAMMED TERRAH [2], RICCARDO TORCHIO [1,3] (Member, IEEE), VINCENZO CIRIMELE [4] (Senior Member, IEEE), LIONEL PICHON [2], MOHAMED BENSETTI [2], AND FABRIZIO DUGHIERO [1]

[1]Department of Industrial Engineering, Università degli Studi di Padova, 35131 Padova, Italy
[2]Génie Électrique et Électronique de Paris, Université Paris-Saclay, CNRS, CentraleSupélec, Sorbonne Université, 91192 Gif-sur-Yvette, France
[3]Department of Information Engineering, Università degli Studi di Padova, 35131 Padova, Italy
[4]Department of Electrical, Electronic, and Information Engineering, University of Bologna, 40136 Bologna, Italy

CORRESPONDING AUTHOR: RICCARDO TORCHIO (email: riccardo.torchio@unipd.it).

ABSTRACT Wireless power transfer (WPT) systems offer a promising solution for automating the charging process and extending the mission duration of unmanned aerial vehicles (UAVs). However, the weight of the WPT system's receiving part mounted on the UAV can significantly impact its energy consumption and overall performance. In this regard, the ferrite plate is a critical component. While it is necessary for improving magnetic coupling and reducing the stray magnetic field, it also increases weight. Topology optimization (TO) is an effective tool for addressing this challenge and identifying the most suitable shape for the ferrite plate. In this study, a multiobjective TO approach based on the solid isotropic material with penalization method is employed to design an optimized ferrite plate for the receiver side of a WPT system for UAV charging. The multiobjective optimization, implemented through a weighted-sum formulation, identifies ferrite configurations that maximize mutual coupling while minimizing material usage. Three representative Pareto-optimal designs are fabricated and experimentally validated against a full-ferrite reference plate. The results show that the reference configuration is a dominated solution in the Pareto sense, as equivalent mutual coupling can be achieved with approximately 40% less ferrite material. The tradeoff between the resulting reduction in charging efficiency and the decrease in the required flight power due to ferrite reduction is analyzed, further demonstrating the potential of TO to substantially reduce system weight without compromising overall system performance.

INDEX TERMS Electromagnetic modeling, inductive power transfer, topology optimization (TO), unmanned aerial vehicles (UAVs), wireless power transfer (WPT).

I. INTRODUCTION

Unmanned aerial vehicles (UAVs), more commonly referred to as drones, are increasingly being adopted in a wide range of fields such as environmental monitoring, precision agriculture, surveillance, and delivery services [1], [2], [3], [4]. Their main advantage is the high level of automation. However, their operational time is limited by battery capacity. Traditional recharging requires the UAV to return to the starting point, reducing mission duration and operational range. To overcome this limitation, recent works proposed the integration of inductive wireless power transfer (WPT) systems into UAVs to automate the charging process [5], [6], [7], [8]. In WPT systems, power transmission is achieved through magnetic coupling between a transmitter (Tx) coil, installed in the charging base, and a receiver (Rx) coil, integrated into the UAV. This enables contactless charging that can easily be automated, making it a particularly flexible and promising solution for UAV applications.

However, several relevant open issues limit the spread of WPT systems in this type of application. In particular, the

© 2026 The Authors. This work is licensed under a Creative Commons Attribution 4.0 License. For more information, see https://creativecommons.org/licenses/by/4.0/

additional weight of the Rx components affects the UAV's energy consumption. Therefore, this weight must be minimized. Another important issue is the alignment of Tx and Rx coils to ensure efficient power transfer. Since perfect positioning is not always achievable when landing the drone, the WPT system must be robust with respect to coil misalignment.

To enhance magnetic coupling between the coils, improve the efficiency of the charging system, and reduce hot spots caused by induced currents in the UAV metallic frame, a ferrite plate is commonly employed both on the Tx and Rx sides, even though this increases the UAV onboard weight [7], [8], [9], [10]. Recent studies have therefore addressed the design of the Rx ferrite plate to achieve a lightweight configuration [11], [12]. All these works adopt bars or tiles as basic units that are then repeated according to fixed geometries or patterns. This approach is based on qualitative assumptions about the magnetic field distribution near the coils. The search for an optimal configuration is therefore limited to adjusting a small set of geometric variables, namely, width, length, height, and spacing pitch. Clearly, this strongly limits the design space and excludes the exploration of unconventional shapes that cannot be identified purely through empirical intuition or prior experience.

Topology optimization (TO) can overcome this limitation by enabling the identification of the optimal material distribution within a given design domain, based on defined objective functions and constraints. In TO, the design domain is divided into discrete elements, each of which is assigned a design variable representing the presence or absence of material. Unlike traditional approaches, TO therefore does not require starting from shapes or distributions of the material imposed a priori, allowing for the discovery of novel and nonintuitive configurations tailored to specific performance goals.

In many practical engineering problems, multiple conflicting objectives must be considered, and the solution is often interpreted in the Pareto sense. TO approaches that account for Pareto-optimal solutions have been implemented in the literature using evolutionary algorithms [13], [14], [15], [16] and gradient-based methods by combining the objective functions into a single weighted-sum formulation, which represents the state-of-the-art method for solving multiobjective TO problems thanks to its simple implementation strategies [17], [18], [19], [20].

While TO has been widely investigated across various engineering fields, its application in electromagnetics has only recently begun to attract significant attention [21], [22], [23], [24], [25]. Naturally, it has drawn increasing interest also for the design of ferrite plates in WPT systems, where it has been applied both in single-objective optimization problems [26], [27], [28], [29] and in multiobjective ones [30], [31]. Focusing on the multiobjective TO, in [30], a genetic algorithm is employed to optimize the ferrite distribution in the magnetic core of a WPT system for electric vehicle applications. Similarly, in [31], a genetic algorithm and a gradient-informed Pareto-based algorithm are applied and compared for multiobjective TO of the ferrite structure in a WPT system, with the aim of maximizing magnetic coupling while minimizing the volume of ferrite material. While these studies provide a thorough analysis and comparison of different optimization algorithms suitable for multiobjective TO in WPT applications, they do not implement the optimized designs nor experimentally validate the results. Furthermore, the WPT systems analyzed in these works are not tailored to a specific target application and, therefore, do not address the constraints associated with a particular use case.

In contrast, the present work explores the application of multiobjective TO to distribute ferrite within the Rx plate of a WPT system specifically designed for UAV charging. The goal is to identify Pareto-optimal solutions maximizing the magnetic coupling between the Tx and Rx coils while minimizing the amount of ferrite used, thereby achieving a lightweight configuration. In addition, a constraint on the Tx self-inductance is incorporated to ensure its stability under misalignment. This requirement arises because WPT systems rely on the resonance with the elements of compensation networks to enhance power transfer efficiency and reduce the volt–ampere rating of the power electronics devices [32]. In case of misalignment, ferrite can affect the magnetic field distribution around the coils causing a variation in Tx and Rx self-inductances and the potential detuning of the resonance condition.

Some of the optimal ferrite configurations obtained through the adopted TO approach are manufactured, and the resulting characteristics are experimentally evaluated. To the best of the authors' knowledge, no previous work in the literature has applied multiobjective TO to the design of the ferrite plate in a WPT system for UAV applications, with subsequent manufacturing of the optimized plates and experimental validation of the numerical results.

The rest of this article is organized as follows. In Section II, a general description of the WPT system for UAV charging considered as the reference for this work is provided. In Section III, the TO concept is briefly recalled, giving particular attention to the approach implemented in the present work. In Section IV, the electromagnetic model implemented for this work and the numerical results from the performed optimization are presented and discussed. Section V describes the experimental validation of the proposed configurations. Finally, Section VI concludes this article and summarizes main outcomes of this work.

II. DEVICE UNDER STUDY

The analysis presented in this article is based on a WPT system specifically designed to operate around the nominal frequency of 150 kHz and to be integrated with a UAV model that operates without additional landing gear [33]. This results in the Tx and Rx coils of the WPT system being positioned in very close proximity so achieving a better magnetic coupling. An image of the computer-aided design (CAD) model of the UAV for which the WPT system was designed is shown in Fig. 1. Further details on the system design and performance can be found in previous works [5], [34], [35].

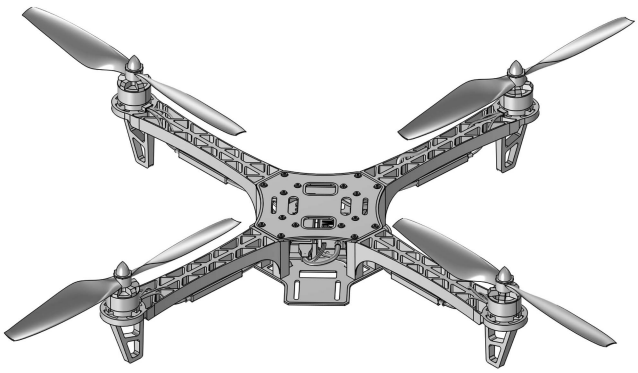

FIGURE 1. Model of the UAV for which the WPT system is designed.

FIGURE 2. Tx coil of the system under study.

The Tx coil, shown in Fig. 2, consists of a circular planar coil with six turns, constructed using litz wire with a diameter of 2.6 mm. The Rx coil also consists of six turns of litz wire, identical to that used in the Tx coil, and also adopts a circular geometry. However, to mitigate the effects of potential misalignment caused by inaccurate UAV positioning during landing, the Rx coil is designed with a diameter equal to half that of the Tx one [5], [36]. A ferrite plate is placed on top of the Rx coil to enhance the coupling between the two coils and serve as shielding to prevent electromagnetic interaction between the Rx coil and the drone landing gear [36]. This ferrite plate is fabricated by bonding 16 tiles, each measuring 25 mm × 25 mm and with a thickness of 2 mm. The ferrite is then attached to a printed circuit board (PCB) on the bottom side of the UAV using a thin adhesive layer. The remaining components of the WPT system, together with the electrical connections between the UAV's motors and their respective electronic drivers, are placed on the top layer of the PCB. Fig. 3 illustrates the Rx assembly, while the main electrical and design parameters of the two assemblies are summarized in Table 1.

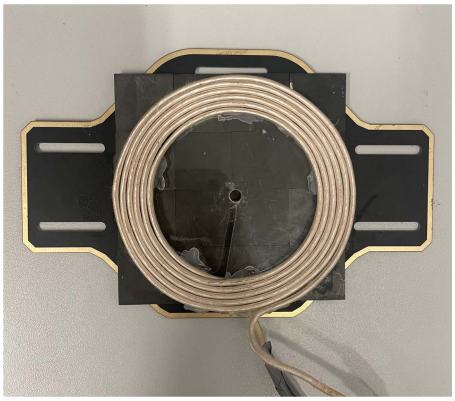

FIGURE 3. Rx coil and Rx ferrite glued on the PCB, taken as reference for the TO.

TABLE 1. Design and Electrical Parameters of the Reference Tx and Rx Assemblies at Nominal Operating Conditions

Parameter	Value
Tx coil external diameter	200 mm
Tx coil number of turns	6
Rx coil external diameter	100 mm
Rx coil number of turns	6
Litz wire number of strands	1000
Litz wire strands diameter	0.05 mm
Litz wire diameter	2.6 mm
Distance between Tx and Rx coils	11 mm
Rx ferrite plate width	105 mm × 100 mm
Rx ferrite plate thickness	2 mm
Ferrite relative permeability	2300
Operating frequency	150 kHz
Nominal power	120 W
Battery voltage	12.6 V
$I_{\mathrm{Tx,RMS}}$	11 A
$I_{\mathrm{Rx,RMS}}$	10.6 A
Tx coil self-inductance	13.08 μH
Rx coil self-inductance	7.66 μH
Mutual inductance	1.18 μH
Tx coil resistance	165 mΩ
Rx coil resistance	80 mΩ

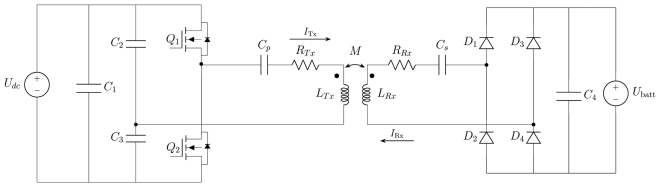

FIGURE 4. Equivalent circuit representation of the WPT system under test.

The system, designed to transfer a rated power of 120 W, can be effectively represented by the equivalent circuit shown in Fig. 4, where Tx and Rx coils are modeled by the inductances L_{Tx} and L_{Rx}, respectively, and their electromagnetic interaction is represented by the mutual inductance M. The

parameters R_{Tx} and R_{Rx} represent the equivalent series resistances of the compensated coils, while the Tx and Rx compensation capacitors are modeled through the capacitances C_p and C_s, respectively.

Series–series compensation has been selected as the compensation topology for this system since the resonance condition is not affected due to the variations in mutual inductance caused by coil misalignment [32], making it well-suited for UAV applications. However, the proximity of the Tx coil to the ferrite plate can still influence the Tx self-inductance under misalignment conditions, leading to mistuning of the compensation network. In particular, previous research [5], [34] has shown that a phase shift between voltage and current at the primary side occurs from 75-mm misalignment conditions, negatively affecting the volt–ampere rating of the source and then the efficiency of the supplying converter. Reducing the amount of ferrite on the Rx plate can then contribute to reducing the weight, but can also help mitigate the variation of the Tx self-inductance under misalignment conditions. On the other hand, reducing the ferrite can negatively affect mutual coupling, which in turn reduces the overall efficiency of the system. Therefore, for this particular application, a multiobjective TO approach is particularly effective in identifying an optimal compromise design.

III. ADOPTED TO APPROACH

TO is a technique that enables the determination of the optimal distribution of a given material within a design domain Ω_d, with the goal of minimizing or maximizing one or more objective functions f_i.

In TO problems, the design domain is discretized and a design variable θ (also called density) is assigned to each element of the mesh. Two main approaches can be defined, based on the mathematical space in which the design variables belong. In the binary approach, the design variable can only assume discrete values, representing the absence or presence of material

$$\theta_i \in \{0, 1\} \quad \forall i = 1 \cdots n \tag{1}$$

where $\theta = 0$ indicates the absence of material and $\theta = 1$ indicates the presence of material.

In contrast, in the continuous approach, the design variable can take any value within the unit interval

$$0 \leq \theta_i \leq 1 \quad \forall i = 1 \cdots n. \tag{2}$$

And it is then correlated with the corresponding material property through a material interpolation scheme (MIS). From a manufacturing perspective, the use of binary design variables is advantageous, as it clearly delineates the regions where material is present or absent. However, the quality of the resulting design heavily depends on the mesh resolution used to discretize the design domain Ω_d. In contrast, using continuous variables allows for higher order interpolation functions, providing greater flexibility [31].

In this study, the solid isotropic material with penalization (SIMP) continuous approach [37] is adopted within Ω_d,

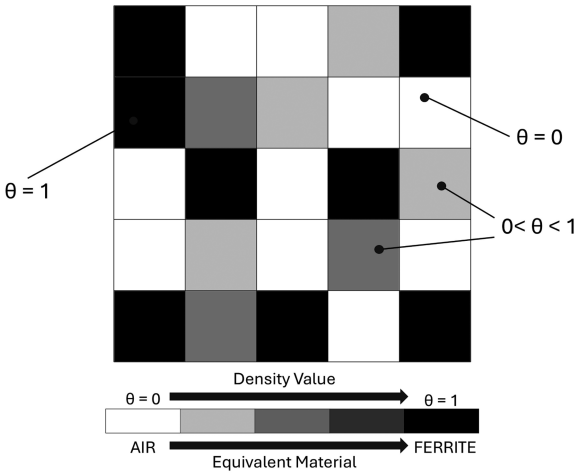

FIGURE 5. Conceptual representation of the SIMP approach.

corresponding to the original Rx ferrite plate volume, such that the material property $\mu_{r,i}$ assigned to the ith element is reconstructed through the following scheme:

$$\mu_{r,i} = \mu_{r,\mathrm{air}} + (\mu_{r,\mathrm{ferrite}} - \mu_{r,\mathrm{air}})\theta_i^{\alpha} \tag{3}$$

where $\mu_{r,\mathrm{air}}$ and $\mu_{r,\mathrm{ferrite}}$ are the relative permeability of air and ferrite, respectively, and α is the penalization parameter. The correspondence between θ_i and the distributed material can be argued from Fig. 5. Similarly to the binary approach, when $\theta_i = 0$, the relative permeability of the element is 1, indicating the absence of ferrite in such element, while $\theta_i = 1$ when the equivalent permeability corresponds to $\mu_{r,\mathrm{ferrite}}$, indicating the presence of ferrite.

The SIMP method is one of the most widely used approaches in TO for WPT systems [24], [28], [38] due to its computational efficiency and relative ease of implementation [39], as the MIS is based on the power law in (3). Consequently, most commercial TO software packages include an implementation of the SIMP technique.

When dealing with continuous TO, since the design variable θ_i is continuous, intermediate values of θ_i result in intermediate permeability values that do not strictly correspond to the presence or absence of material. One of the main challenges is then the presence of these intermediate material densities in the optimal design, since their physical interpretation in terms of real materials is not always straightforward. The SIMP method provides an important advantage in this context by introducing a penalization strategy through the choice of the α parameter in (3), which reduces intermediate densities and guides the solution toward designs that are more physically meaningful.

In this work, numerical techniques, such as the Helmholtz filter and the hyperbolic tangent projection, are also applied at each iteration to mitigate this so-called "grayscale" phenomenon, as discussed in [21], [40]. Specifically, in the Helmholtz filtering stage, the filter radius was set equal to the maximum element size of the mesh in the design domain, while for the hyperbolic tangent projection, a projection slope

of $\beta = 8$ and a projection point of $\theta_b = 0.5$ were used. Finally, a value of $\alpha = 7$ was adopted. Furthermore, at the end of the optimization, all elements with $\theta_i > 0.5$ are assigned to ferrite.

It is worth noting that, being the number of decision variables equal to the number of finite elements discretizing Ω_d, TO falls into the class of large-scale optimization problems. As a result, TO is typically solved using gradient-based methods, as the high dimensionality of the design space can quickly lead to the curse of dimensionality [41]. Gradient-based optimization techniques applicable to such constrained problems often require transforming the multiobjective optimization problem into a single-objective formulation [42]. In this work, the two objective functions $f_1(\theta)$, representing the mutual inductance, and $f_2(\theta)$, representing the amount of ferrite material in the Rx plate, are combined into a single-objective function $f(\theta)$ using the weighted sum approach through the weights w_1 and w_2. The resulting constrained optimization problem can be expressed as

$$\begin{aligned} \max \left\{ f(\theta) = w_1 f_1(\theta) - w_2 f_2(\theta) = w_1 \frac{M_0(\theta)}{M_{\text{full}}} - w_2 \frac{V(\theta)}{V_{\text{full}}} \right\} \\ \text{with} \quad w_1 + w_2 = 1 \\ \text{subject to} \quad 0.95\, L_0(\theta) \leq L_{75}(\theta) \leq 1.05\, L_0(\theta) \end{aligned} \tag{4}$$

where $M_0(\theta)$ represents the mutual inductance subject to the TO material distribution at 0-mm misalignment, and M_{full} is the mutual inductance with the reference plate at 0 mm. $V(\theta)$ is the actual volume of material distributed in Ω_d, while V_{full} is the entire volume of Ω_d. It is worth noting that maximizing $f(\theta)$ corresponds to maximizing the mutual inductance while simultaneously minimizing the amount of ferrite material within the design domain. Regarding the constraint, it ensures that the self-inductance of the Tx coil at 75-mm misalignment, indicated as L_{75}, remains within $\pm 5\%$ of its value at perfect alignment, indicated as L_0. This level of variation is considered acceptable, as it falls within the usual tolerance range of commercially available capacitors [43]. During the optimization process, L_{75} and L_0 are evaluated at each iteration, verifying that L_{75} remains within the bounds specified in (4). The constraint is handled through a penalization factor; therefore, solutions that do not satisfy it are not automatically discarded. As a result, certain solutions may not fully comply with the constraint.

The Pareto front representing the set of optimal solutions is obtained by performing multiple optimizations varying the weights in (4). Since the weights w_1 and w_2 must sum to one, the remainder of this article will refer only to w_1, assuming that $w_2 = 1 - w_1$. In particular, the Pareto front is approximated using ten optimization points obtained by linearly sweeping w_1 from 0 to 1.

IV. ELECTROMAGNETIC MODELING AND NUMERICAL RESULTS

In this work, the TO process is performed using the finite-element method (FEM). Specifically, the optimization module of the commercial software COMSOL Multiphysics is employed, where the SIMP approach is implemented. Since each optimization iteration requires evaluating the mutual inductance at 0-mm misalignment as well as L_{75} and L_0, the model was designed to account for both misalignment conditions within a single iteration by including two Tx coils in the geometry. These coils were alternatively excited in separate solver steps by prescribing the appropriate current density in the active coil while assigning air properties to the inactive one. This choice, combined with the large number of design variables in TO, makes the problem computationally demanding. Therefore, it is crucial to adopt strategies that reduce the overall computational effort. In the FEM model, a simplified equivalent representation of the Rx and Tx coils as homogeneous conductors with uniform current density is used to reduce complexity [44]. In addition, geometric symmetry along one axis is exploited. The geometry of the model implemented to perform the optimization is shown in Fig. 6.

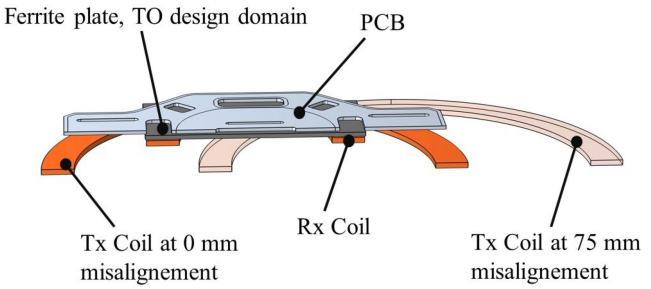

FIGURE 6. Geometry implemented to perform the TO.

The problem is treated as a magneto quasi-static problem and solved via the magnetic vector potential **A** formulation. To further simplify the model, the conductive PCB located above the ferrite is treated as a perfectly electrically conductive (PEC) material by adopting a boundary condition that forces the magnetic flux density **B** to be tangential to its surface. This PEC assumption is considered appropriate for modeling the device, given the presence of the large ground plane that characterizes the PCB. This approach accounts for the PCB's influence on mutual coupling due to induced currents, without requiring a too fine mesh resolution to accurately capture the skin effect. Particular attention is also given to the discretization of the TO design domain, as it directly affects the optimization process. A structured quadrilateral mesh with 5 mm × 5 mm elements is first generated and converted into a triangular mesh by splitting each quadrilateral along its diagonal. The resulting mesh is then extruded through the thickness to obtain a hexahedral volume mesh. Finally, the magnetic behavior of the ferrite is assumed to be linear. This approximation is justified by preliminary analyses of the WPT system prior to optimization, which show that the maximum magnetic flux density induced in the ferrite plate under standard operating conditions is approximately 35 mT [5].

The optimization is performed on a workstation equipped with an Intel Xeon processor (16 cores, 3.10 GHz) and

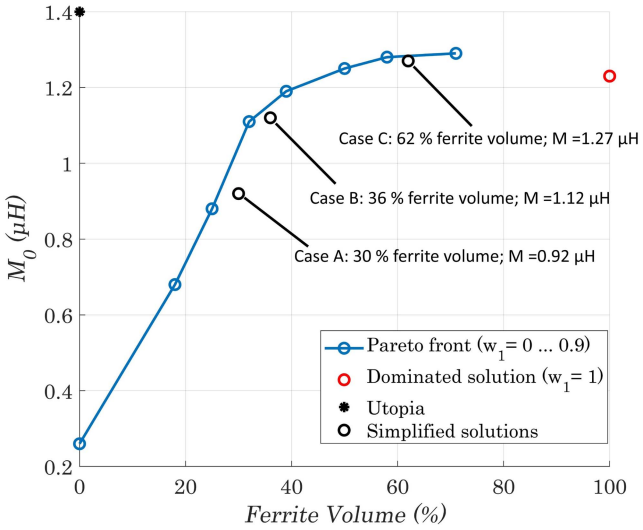

FIGURE 7. Pareto front obtained through the weighted sum approach. The solution with full material is a dominated solution. The black dots represent the manufactured solutions.

TABLE 2. Simulated Values of M_0, Ferrite Material Percentage, Tx Self-Inductance Under Misalignment Conditions and Relative Difference in M_0 for Different Weight Values

w_1	Ferrite volume	M_0	ΔL_{Tx}	ΔM
0	0%	0.26 μH	5%	-78%
0.1	0%	0.26 μH	5%	-78%
0.2	0%	0.26 μH	5%	-78%
0.3	18%	0.68 μH	4%	-44%
0.4	25%	0.88 μH	5%	-28%
0.5	32%	1.11 μH	5%	-10%
0.6	39%	1.19 μH	5%	-3%
0.7	50%	1.25 μH	6%	+1.5%
0.8	58%	1.28 μH	10%	+4%
0.9	71%	1.29 μH	11%	+5%
1	100%	1.23 μH	12%	-

128 GB of RAM. The computation time for each set of weights is approximately 13 h.

The obtained Pareto front is shown in Fig. 7, while the corresponding values of mutual inductance at 0-mm misalignment conditions M_0 and ferrite material percentage are summarized in Table 2. In addition, the table reports the relative difference in mutual inductance between each optimized solution and the reference configuration $\Delta M = (M_{\mathrm{full}} - M_0)/M_{\mathrm{full}}$ (in percent), along with the relative variation in Tx self-inductance between the 75- and the 0-mm misalignment conditions for each optimized plate $\Delta L_{\mathrm{Tx}} = (L_{75} - L_0)/L_0$ (in percent).

It is particularly interesting to note that the full-material solution, i.e., the reference plate configuration, is a dominated solution in the Pareto sense, as it presents a lower mutual inductance while using more ferrite material compared to other optimized solutions. Moreover, it is important to observe that the variation in the Tx self-inductance due to misalignment remains within the prescribed 5% range for solutions in which the ferrite usage remains below 39%, thereby satisfying the imposed constraint. For configurations with greater ferrite quantity, the constraint is no longer strictly satisfied.

The corresponding ferrite shapes resulting from the TO, which represent the points on the Pareto front for the different weights, are reported in Fig. 8. The configurations obtained with $w_1 = 0$ and $w_1 = 1$ are not included, as they correspond to trivial cases: the absence of ferrite and the fully filled reference plate, respectively. By analyzing the obtained optimized shapes, it can be observed that material removal from a given region indicates a limited contribution to magnetic flux guidance and, consequently, a negligible impact on system performance. This behavior is particularly evident in the central region, where ferrite is removed in all configurations, as the magnetic flux density is nearly zero and therefore does not influence the mutual inductance. This result is consistent with expectations and has also been reported in previous studies [29], [45].

It is evident that the final shapes generated by the TO are challenging to manufacture due to their irregular and complex geometries. Therefore, to ensure practical feasibility, the optimized shapes must be simplified prior to fabrication. Among the set of Pareto-optimal solutions, three representative configurations were selected and simplified for manufacturing and experimental validation. Specifically, the solution corresponding to $w_1 = 0.4$ was chosen for its ease of machinability. The configuration with $w_1 = 0.5$ was selected because it satisfies the constraint on the Tx self-inductance while achieving a significant reduction in ferrite volume, with only a 10% decrease in mutual inductance compared to the reference case. Finally, the solution corresponding to $w_1 = 0.8$ was included to demonstrate that a reduced amount of ferrite can yield a higher mutual inductance than the reference plate.

In the remainder of this article, the simplified geometries associated with $w_1 = 0.4$, $w_1 = 0.5$, and $w_1 = 0.8$ are referred to as Cases A–C, respectively. The simplified geometries are shown alongside the original TO results in Figs. 9–11 for Cases A–C, respectively. The adopted simplification was driven by the need to obtain manufacturable geometries that favor straight cuts and avoid sharp corners and jagged edges, thereby enabling machining, especially in a laboratory-scale setting. A quantitative comparison of the simulated differences in mutual inductance, ferrite volume, and ΔL_{Tx} between the original optimized designs and the corresponding simplified geometries is reported in Table 3. Moreover, the differences between the original and simplified shapes are highlighted in Fig. 7, where the simplified geometries are also reported.

V. EXPERIMENTAL VALIDATION

The manufactured three simplified geometries derived from the TO results are shown in Fig. 12. Each ferrite plate has been manufactured by cutting the individual tiles using a diamond wire saw.

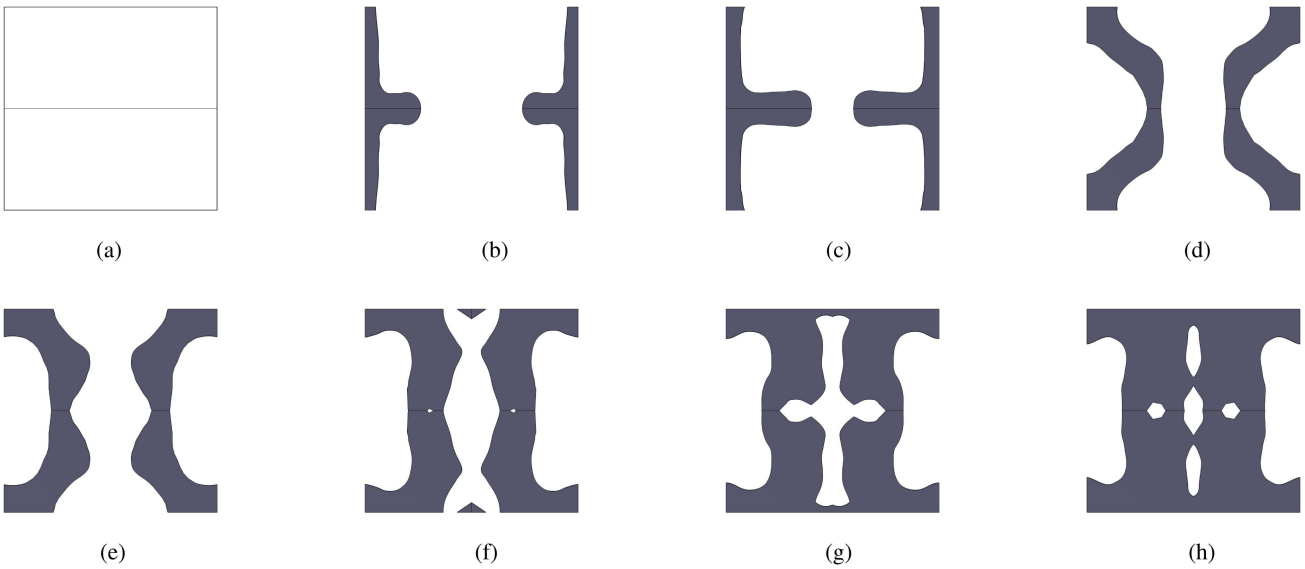

FIGURE 8. Ferrite shapes resulting from the TO multiobjective optimization. (a) $w_1 = 0.1$, $w_1 = 0.2$. (b) $w_1 = 0.3$. (c) $w_1 = 0.4$. (d) $w_1 = 0.5$. (e) $w_1 = 0.6$. (f) $w_1 = 0.7$. (g) $w_1 = 0.8$. (h) $w_1 = 0.9$.

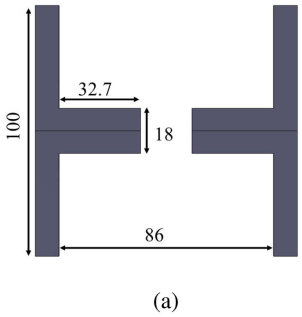

FIGURE 9. Optimized ferrite plate for Case A. (a) Simplified shape. (b) Original from TO. Units in millimeter

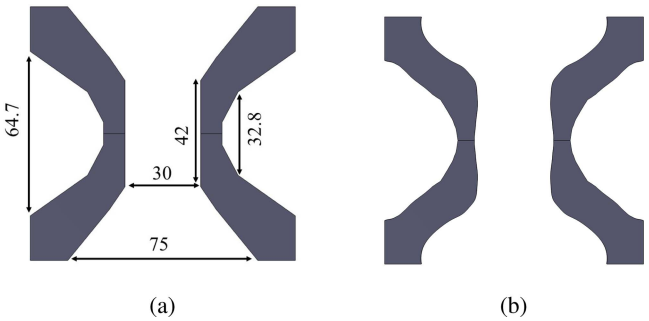

FIGURE 10. Optimized ferrite plate for Case B. (a) Simplified shape. (b) Original from TO. Units in millimeter.

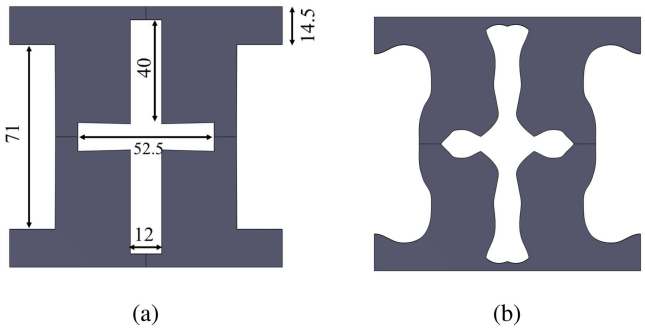

FIGURE 11. Optimized ferrite plate for Case C: simplified shape (a) and original from TO (b). Units in mm.

TABLE 3. Simulated Values of M_0, Ferrite Material Percentage, and ΔL_{Tx} for the Original Optimized Designs and the Corresponding Simplified Geometries

Case	Ferrite volume	M_0	ΔL_{Tx}
A	30%	0.92 μH	5%
A original from TO	25%	0.88 μH	5%
B	36%	1.12 μH	4%
B original from TO	32%	1.11 μH	5%
C	62%	1.27 μH	11%
C original from TO	58%	1.28 μH	10%

The self and mutual inductance values of the coils for each assembly are measured using a Wayne Kerr 4300 series *LCR* meter at the operating frequency and under the same injected current. The measured values are reported in Table 4 together with the corresponding simulation results. Table 4 also reports the measured values of mutual inductance, where ΔM denotes the relative difference between each optimized plate and the reference configuration, while Table 5 summarizes the measured relative variation in Tx self-inductance under misalignment conditions for each optimized plate. An example of the system employed for these tests is illustrated in Fig. 13.

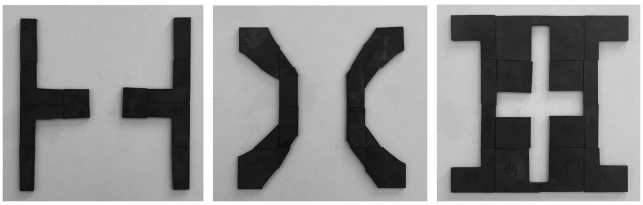

(a) (b) (c)

FIGURE 12. Manufactured ferrite plates. (a) Case A. (b) Case B. (c) Case C.

TABLE 4. Comparison Between Measured Mutual Inductance and Simulated One. ΔM Represents the Relative Variation With Respect to the Reference Case

Case	A	B	C	Reference
Ferrite volume	30%	36%	62%	100%
M_0 **measured**	0.90 μH	1.07 μH	1.18 μH	1.18 μH
M_0 **simulated**	0.92 μH	1.12 μH	1.27 μH	1.23 μH
Relative Error	2%	5%	7.5%	4%
ΔM	-23%	-9%	0%	-

TABLE 5. Comparison Between Measured Tx Self-Inductance Variations and Simulated Ones

Case	A	B	C	Reference
Ferrite volume	30%	36%	62%	100%
ΔL_{Tx}**measured**	5%	4%	5%	9%
ΔL_{Tx}**simulated**	5%	4%	11%	11%
Relative Error	-	-	6%	3%

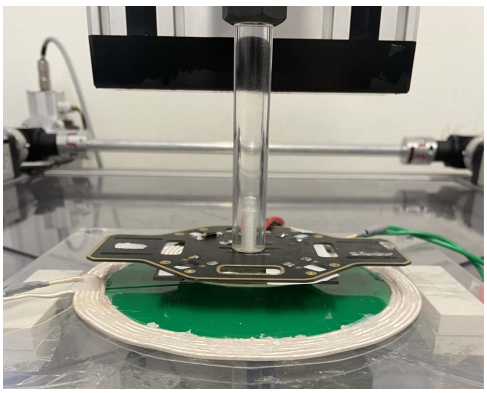

FIGURE 13. System under test.

As observed in both Tables 4 and 5, the experimental results show good agreement with the numerical simulations. Minor discrepancies can be attributed to modeling approximations, particularly in the conductor representation, as well as to tolerances in coil placement during measurements and, most notably, machining tolerances in the manufacturing of the ferrite shapes. Furthermore, although Case C does not exhibit a mutual inductance value higher than that of the reference configuration, it is worth noting that the measured value of M_0 in that case is identical to that of the reference plate. This

TABLE 6. Measured Values of L_{Tx} and L_{Rx}, M and k Under Perfect Alignment and 75-mm Misalignment Conditions

Case	A	B	C	Reference
Ferrite volume	30%	36%	62%	100%
M_0 **measured**	0.90 μH	1.07 μH	1.18 μH	1.18 μH
$L_{Tx,0}$ **measured**	13 μH	13.07 μH	13.05 μH	13.08 μH
$L_{Rx,0}$ **measured**	5.42 μH	6.20 μH	6.61 μH	7.66 μH
k_0	0.11	0.12	0.13	0.12
M_{75} **measured**	0.77 μH	0.89 μH	1.08 μH	1.1 μH
$L_{Tx,75}$ **measured**	13.63 μH	13.66 μH	14.01 μH	14.37 μH
$L_{Rx,75}$ **measured**	5.37 μH	6.22 μH	6.53 μH	7.77 μH
k_{75}	0.09	0.096	0.11	0.10

TABLE 7. Measured Values of Rx Resistance

Case	Ferrite volume	Rx resistance	ΔR_{Rx}
A	30%	167 mΩ	108%
B	36%	130 mΩ	62%
C	62%	95 mΩ	19%
Reference	100%	80 mΩ	-

confirms that the reference case is a dominated solution in the Pareto sense, demonstrating that a significant reduction in ferrite material can be achieved without compromising magnetic coupling performance. Regarding the variation in Tx self-inductance, it is evident that all three tested cases successfully maintain the variation within the acceptable limit defined by the system constraints. To provide a more comprehensive characterization of the system behavior with the proposed ferrite plates, the measured values of the Tx and Rx self-inductances, together with the mutual inductance M and the coupling coefficient k, are reported for both perfect alignment and 75-mm misalignment conditions in Table 6. It is worth noting that Case C exhibits a higher coupling coefficient than the full-ferrite reference configuration under both alignment conditions.

When reducing the ferrite volume, it is also important to note that the current density distribution in the Rx coil is affected by the proximity effect with the conductive parts of the PCB. This phenomenon becomes more pronounced as the amount of ferrite decreases. Therefore, to provide a more comprehensive assessment of the impact of the optimized ferrite plates on the system, the Rx coil resistance is measured with an *LCR* meter at the working frequency for the different configurations and compared to the reference case. The measured resistance values are reported in Table 7, along with the corresponding relative increases compared to the reference configuration. As observed, reducing the ferrite volume results in a substantial increase in coil resistance, which negatively affects the overall system efficiency.

The DC–DC efficiency under perfect alignment, denoted as η_0, is reported in Table 8 together with the corresponding reduction in the required flight power, denoted as ΔP_{f}. The efficiency is evaluated under the same transferred power at the load for all cases. This is obtained by regulating the input DC voltage (i.e., the voltage U_{dc} in Fig. 4).

TABLE 8. Transmission Efficiency and Reduction in the Required Flight Power

Case	η_0	ΔP_f
A	60%	15%
B	69%	14%
C	75%	8%
Reference	77%	-

P_f is the power required for an UAV to remain in flight. As demonstrated in [46], this power is proportional to the total UAV mass m, according to the relationship $P_f \propto m^{3/2}$. The reduction in the required flight power, ΔP_f, resulting from the ferrite volume reduction achieved through the proposed TO is computed as

$$\Delta P_f = 1 - \left(\frac{m_{tk} + m_{fc}}{m_{tk} + m_f} \right)^{3/2} \tag{5}$$

where $m_{tk} = 800\,\text{g}$ is the UAV takeoff mass without the WPT system [33], $m_f = 135\,\text{g}$ is the mass of the reference ferrite plate [34], and m_{fc} represents the ferrite mass for Cases A–C.

It can be appreciated that Case C, which achieves approximately a 40% reduction in ferrite volume, corresponds to an 8% reduction in the required flight power, while maintaining the same mutual coupling as the full-ferrite reference configuration. In addition, it presents a reduced variation of the Tx self-inductance under misalignment conditions by 5%, resulting in a higher coupling coefficient than the full-ferrite reference configuration under both alignment conditions. Despite an increase in the Rx coil resistance of less than 20%, which leads to an efficiency reduction of only 2%, this solution represents a well-balanced tradeoff for the proposed application.

VI. CONCLUSION

This article presented the application of a dedicated TO technique for the design of the ferrite plate in the Rx assembly of a WPT system intended for UAV charging. In this study, the TO problem is formulated as a multiobjective optimization, with the goal of minimizing the amount of ferrite material used in the Rx side while maximizing the mutual coupling between the coils. These two objectives are combined into a single-objective function using the weighted sum approach, and the optimal solutions are described in the Pareto sense. To make the proposed solutions feasible with the application requirements, a constraint on the variation of the Tx coil self-inductance is also set. The main outcome of this work is demonstrating the feasibility of employing multiobjective TO as a tool for the design of WPT systems for UAVs, enabling lighter designs while maintaining high performance.

Among the various configurations obtained, three are selected for manufacturing, and the simulation results are subsequently validated through experimental measurements. A key outcome of this work is also the confirmation that the full-ferrite solution can be a dominated configuration in the Pareto sense with respect to the two objective functions under consideration. In particular, for the case under study, the same level of magnetic coupling achieved by the full-ferrite configuration can be maintained while reducing the ferrite material by approximately 40%. This result is particularly relevant for UAV applications where reduction of weight is a key objective. It is clearly worth underlining that, although the proposed methodology is general, the optimized design is inherently tailored to the specific system under study, and variation in geometrical parameters of the coil could result in a different geometry. The experimental results on the optimized systems also revealed that reducing the ferrite material increases the Rx coil resistance, thereby affecting the overall system efficiency. In the present work, efficiency was not included among the objective functions, as the focus was on minimizing weight while preserving magnetic coupling. Clearly, the efficiency degradation associated with increased Rx resistance can be mitigated by adopting litz wires with smaller strand diameters. Nevertheless, for applications where efficiency is a priority, future research could focus on incorporating the resistance evaluation directly into the optimization process.

Finally, although thermal effects were not considered in this study, losses can lead to heating and potential thermal management challenges. These effects are another important parameter to investigate in future work, especially for higher power applications.

In addition, the proposed optimized designs consider only static misalignment conditions; however, practical WPT operation is also affected by dynamic variations of system parameters. Future work could investigate integrating recent recursive parameter identification techniques into WPT systems to track these variations and enhance the robustness of the optimized Rx designs under real-world operating conditions.

REFERENCES

[1] S. M. S. M. Daud et al., "Applications of drone in disaster management: A scoping review," *Sci. Justice*, vol. 62, no. 1, pp. 30–42, 2022.

[2] F. Toscano et al., "Unmanned aerial vehicle for precision agriculture: A review," *IEEE Access*, vol. 12, pp. 69188–69205, 2024.

[3] A. Gohari, A. B. Ahmad, R. B. A. Rahim, A. S. M. Supa'at, S. A. Razak, and M. S. M. Gismalla, "Involvement of surveillance drones in smart cities: A systematic review," *IEEE Access*, vol. 10, pp. 56611–56628, 2022.

[4] A. Rejeb, K. Rejeb, S. J. Simske, and H. Treiblmaier, "Drones for supply chain management and logistics: A review and research agenda," *Int. J. Logistics Res. Appl.*, vol. 26, no. 6, pp. 708–731, 2023.

[5] M. Terrah, M.-K. Smail, L. Pichon, and M. Bensetti, "Parametric design approach for wireless power transfer system: UAV applications," *Drones*, vol. 8, no. 12, Dec. 2024, Art. no. 735.

[6] Z. Bie, J. Zhang, K. Song, D. Wang, and C. Zhu, "A free-rotation asymmetric magnetic coupling structure of UAV wireless charging platform with conformal pickup," *IEEE Trans. Ind. Electron.*, vol. 69, no. 10, pp. 10154–10161, Oct. 2022.

[7] W. Huang, X. Yan, W. Chen, F. Zhu, Y. Yang, and Y. Zhang, "Magnetic structure design for drone WPT with ultra-low stray magnetic fields and high anti-offset performance," *IEEE Trans. Ind. Electron.*, vol. 73, no. 2, pp. 2059–2068, Feb. 2026.

[8] J. Wang, R. Chen, C. Cai, J. Zhang, and C. Wang, "An onboard magnetic integration-based WPT system for UAV misalignment-tolerant

charging with constant current output," *IEEE Trans. Transport. Electrific.*, vol. 9, no. 1, pp. 1973–1984, Mar. 2023.
[9] X. Li, J. Lu, and S. Stegen, "Magnetic coupler optimization for inductive power transfer system of unmanned aerial vehicles," *Energies*, vol. 14, no. 21, Oct. 2021, Art. no. 7024.
[10] S. Wu, C. Cai, X. Liu, W. Chai, and S. Yang, "Compact and free-positioning omnidirectional wireless power transfer system for unmanned aerial vehicle charging applications," *IEEE Trans. Power Electron.*, vol. 37, no. 8, pp. 8790–8794, Aug. 2022.
[11] Z. Xie, Q. Wang, B. Wen, J. Zhao, W. Xiao, and B. Zhang, "Design method of magnetic coupling mechanism for UAV wireless charging system with high efficiency and anti-offset ability," in *Proc. 2nd China Power Supply Soc. Electromagn. Compat. Conf.*. Hangzhou, China, Aug. 2024, pp. 258–263.
[12] F. Rosu and A. Badescu, "Electric and magnetic design of a deployable WPT system for industrial and defense UAV applications," *Electronics*, vol. 10, no. 18, Sep. 2021, Art. no. 2252.
[13] D. Guirguis and M. F. Aly, "An evolutionary multi-objective topology optimization framework for welded structures," in *Proc. IEEE Congr. Evol. Comput.*. Vancouver, BC, Canada, Jul. 2016, pp. 372–378.
[14] T. Kunakote and S. Bureerat, "Multi-objective topology optimization using evolutionary algorithms," *Eng. Optim.*, vol. 43, no. 5, pp. 541–557, May 2011.
[15] Y. Li, L. Liu, S. Yang, Z. Ren, and Y. Ma, "A multi-objective topology optimization methodology and its application to electromagnetic actuator designs," *IEEE Trans. Magn.*, vol. 56, no. 2, Feb. 2020, Art. no. 7506004.
[16] S. Doi, H. Sasaki, and H. Igarashi, "Multi-objective topology optimization of rotating machines using deep learning," *IEEE Trans. Magn.*, vol. 55, no. 6, Jun. 2019, Art. no. 7202605.
[17] J. Wang, D. Melideo, X. Liu, and U. Desideri, "Comparative study on topology optimization of microchannel heat sink by using different multi-objective algorithms and objective functions," *Appl. Thermal Eng.*, vol. 252, Sep. 2024, Art. no. 123606.
[18] H. L. Simonetti, V. S. Almeida, F. De Assis Das Neves, and M. Greco, "Multi-objective topology optimization using the boundary element method," *Structures*, vol. 19, pp. 84–95, Jun. 2019.
[19] J. Wang, U. Desideri, and X. Liu, "Multi-objective structure optimization and performance analysis of catalytic micro-reactor channel designed by an improved topology optimization model," *Appl. Thermal Eng.*, vol. 244, May 2024, Art. no. 122742.
[20] D. Huang, S. Zhou, and X. Yan, "Multi-objective topology optimization design of thermal-mechanical coupling structure based on FPTO method," *Optim. Eng.*, vol. 26, no. 1, pp. 53–81, Mar. 2025.
[21] F. Lucchini, R. Torchio, V. Cirimele, P. Alotto, and P. Bettini, "Topology optimization for electromagnetics: A survey," *IEEE Access*, vol. 10, pp. 98593–98611, 2022.
[22] Y. Otomo and H. Igarashi, "Topology optimization using Gabor filter: Application to synchronous reluctance motor," *IEEE Trans. Magn.*, vol. 57, no. 6, Jun. 2021, Art. no. 8203004.
[23] T. Cherrière et al., "Multi-material topology optimization using Wachspress interpolations for designing a 3-phase electrical machine stator," *Struct. Multidisciplinary Optim.*, vol. 65, no. 12, Dec. 2022, Art. no. 352.
[24] F. Lucchini, R. Torchio, P. Bettini, and F. Dughiero, "TopIE: An integral equation tool for topology optimization in electromagnetics," *IEEE Trans. Antennas Propag.*, vol. 72, no. 1, pp. 683–692, Jan. 2024.
[25] M. Yin, M. Naidjate, N. Bracikowski, A. Pierquin, and D. Trichet, "Topology optimization of non-linear electromagnetic actuator based on reluctance network analysis," *J. Magnetism Magn. Mater.*, vol. 602, Jul. 2024, Art. no. 172174.
[26] C. Lee, "Topology optimization of the transmitter ferrite and receiver coil for minimizing the weight of the wireless-charging portable devices," *IEEE Trans. Ind. Electron.*, vol. 71, no. 10, pp. 12192–12201, Oct. 2024.
[27] Y. Otomo and H. Igarashi, "A 3-D topology optimization of magnetic cores for wireless power transfer device," *IEEE Trans. Magn.*, vol. 55, no. 6, Jun. 2019, Art. no. 8103005.
[28] Y. Pei, L. Pichon, Y. L. Bihan, and M. Bensetti, "SIMP-Method topology optimization of ferrite structures in inductive power transfer systems," *IEEE Trans. Electromagn. Compat.*, vol. 65, no. 6, pp. 1744–1750, Dec. 2023.
[29] G. Poggiana et al., "Single objective topology optimization and experimental validation of a VA ferrite plate for a SAE-Compliant WPT system," *IEEE Trans. Transp. Electrific.*, early access, 26 Jan. 2026, doi: 10.1109/TTE.2026.3651913.
[30] Y. Otomo and H. Igarashi, "Topology optimization of magnetic cores for WPT using the geometry projection method," *Int. J. Comput. Math. Elect. Electron. Eng.*, vol. 41, no. 3, pp. 889–899, 2022.
[31] F. Lucchini, R. Torchio, and P. Alotto, "Gradient-informed Pareto-based multi-objective binary topology optimization," *IEEE Access*, vol. 13, pp. 86576–86587, 2025.
[32] F. Corti, V. Bertolini, A. Faba, E. Cardelli, and A. Reatti, "Design procedures for series–series WPT systems: A comparative analysis," *Comput. Elect. Eng.*, vol. 119, 2024, Art. no. 109511.
[33] F450 User Manual, DJI Technology Co., Ltd., May 2015. [Online]. Available: https://dl.djicdn.com/downloads/flamewheel/en/F450_User_Manual_v2.2_en.pdf
[34] M. Terrah, M.-K. Smail, L. Pichon, M. Bensetti, and A. Goudjil, "Multi-objective optimization of a WPT system for UAVs," in *Proc. Int. Symp. Electromagn. Compat.*, 2025, pp. 948–952.
[35] W. Rischebé, M. Terrah, L. Pichon, M. K. Smail, and M. Bensetti, "Multi-objective optimization of a wireless power transfer system for UAV," *J. Electromagn. Waves Appl.*, pp. 1–12, Dec. 2025.
[36] V. Cirimele, R. Mandrioli, R. Torchio, G. Gentile, F. Giulietti, and G. Grandi, "Design considerations on modular WPT charging systems for drones in civil applications," in *Proc. Int. Conf. Clean Elect. Power*, Terrasini, Italy, Jun. 2023, pp. 452–457.
[37] O. Sigmund and K. Maute, "Topology optimization approaches: A comparative review," *Struct. Multidisciplinary Optim.*, vol. 48, no. 6, pp. 1031–1055, Dec. 2013.
[38] G. Poggiana, R. Torchio, V. Cirimele, and F. Dughiero, "Topology optimization of a VA plate for SAE-compliant wireless power transfer system using anisotropic SMC materials," in *Proc. IEEE Wirel. Power Technol. Conf. Expo.*, Rome, Italy, Jun. 2025, pp. 1–5.
[39] S. Sanogo and F. Messine, "Topology optimization in electromagnetism using SIMP method: Issues of material interpolation schemes," *Int. J. Comput. Math. Elect. Electron. Eng.*, vol. 37, no. 6, pp. 2138–2157, Nov. 2018.
[40] F. Wang, B. S. Lazarov, and O. Sigmund, "On projection methods, convergence and robust formulations in topology optimization," *Struct. Multidisciplinary Optim.*, vol. 43, no. 6, pp. 767–784, Jun. 2011.
[41] O. Sigmund, "On the usefulness of non-gradient approaches in topology optimization," *Struct. Multidisciplinary Optim.*, vol. 43, no. 5, pp. 589–596, May 2011.
[42] K. Izui, T. Yamada, S. Nishiwaki, and K. Tanaka, "Multiobjective optimization using an aggregative gradient-based method," *Struct. Multidisciplinary Optim.*, vol. 51, no. 1, pp. 173–182, Jan. 2015.
[43] V. Cirimele et al., "Uncertainty quantification for SAE J2954 compliant static wireless charge components," *IEEE Access*, vol. 8, pp. 171489–171501, 2020.
[44] R. Bosshard, U. Iruretagoyena, and J. W. Kolar, "Comprehensive evaluation of rectangular and double-D coil geometry for 50 kW/85 kHz IPT system," *IEEE Trans. Emerg. Sel. Top. Power Electron.*, vol. 4, no. 4, pp. 1406–1415, Dec. 2016.
[45] M. Bensetti, K. Kadem, Y. Pei, Y. Le Bihan, E. Labouré, and L. Pichon, "Parametric optimization of ferrite structure used for dynamic wireless power transfer for 3kW electric vehicle," *Energies*, vol. 16, no. 14, Jul. 2023, Art. no. 5439.
[46] E. L. De Angelis, F. Giulietti, G. Rossetti, and G. Bellani, "Performance analysis and optimal sizing of electric multirotors," *Aerosp. Sci. Technol.*, vol. 118, Nov. 2021, Art. no. 107057.

GIULIO POGGIANA received the M.Sc. degree in electrical energy engineering in 2023 from the University of Padova, Padua, Italy, where he is currently working toward the Ph.D. degree in electrical engineering.

From February to July 2025, he was a visiting Ph.D. student with the Laboratoire de Génie Électrique de Paris, Paris, France. His research interests include wireless power transfer, electromagnetic modeling and simulation, and induction heating.

MOHAMMED TERRAH received the M.Sc. degree in electrical engineering with a focus on the physics and engineering of energy from Paris-Saclay University, Paris, France, in 2022, and the Engineering degree in electrical engineering with a focus on electrical machines from the Higher School of Electrical and Energetic Engineering, Oran, Algeria, in 2021. He is currently working toward the Ph.D. degree in electrical engineering with Paris-Saclay University.

His research focuses on wireless power transfer systems for unmanned aerial vehicle applications.

RICCARDO TORCHIO (Member, IEEE) was born in Padua, Italy, in 1992. He received the M.S. degree in electrical engineering from the University of Padova, Padua, in 2016, and the dual Ph.D. degree in electrical engineering from the University of Padova and Grenoble Electrical Engineering Laboratory, Universitè Grenoble Alpes, Saint-Martin-d'Hères, France, in 2019.

He is currently an Assistant Professor (RTDb) with the University of Padova. His research interests include numerical methods, optimizations, low-rank compression techniques, uncertainty quantifications, wireless power transfer applications, model order reduction, model-predictive control, and the development of integral formulations for the study of low- and high-frequency electromagnetic devices.

VINCENZO CIRIMELE (Senior Member, IEEE) received the M.Sc. (summa cum laude) and Ph.D. degrees in electrical engineering from the Politecnico di Torino, Turin, Italy, in 2013 and 2017, respectively, and the Ph.D. (Hons.) degree in electronics engineering from the Université Paris Saclay, Gir-sur-Yvette, France, in 2017.

He is currently an Associate Professor with the Department of Electrical, Electronic, and Information Engineering, Alma Mater Studiorum University of Bologna, Bologna, Italy. From 2020 to 2021, he was a Technical Responsible for the R&D and Innovation Group of the company Movyon S.p.A., Florence, Italy, of Autostrade per l'Italia Group, where he supervised projects related to energy sustainability and development of highway electric mobility. From 2017 to 2020, he was an Assistant Professor with the Department of Energy, Politecnico di Torino. His research interests include technologies for electric mobility, inductive power transmission, electromagnetic modeling and simulation, and power electronics.

Dr. Cirimele is a Deputy Editor for *IET Power Electronics* and an Associate Editor for IEEE TRANSACTION ON TRANSPORTATION ELECTRIFICATION and *Wireless Power Transfer*.

LIONEL PICHON received the Dip. Eng. degree in electrical engineering from Ecole Supérieure d'Ingénieurs en Electronique et Electrotechnique (ESIEE-Paris), Noisy-le-Grand, France, in 1984, and the Ph.D. degree in electrical engineering from Laboratoire de Génie Electrique de Paris, Gif-sur-Yvette, France, in 1989.

He is currently a Senior Researcher (Directeur de recherche) with the Group of Electrical Engineering of Paris (GeePs), CNRS (French National Centre for Scientific Research), Paris, France. In 1985, he joined the Laboratoire de Génie Electrique de Paris (LGEP, now GeePs). He is the author or coauthor of more than 130 journal articles in peer-reviewed journals. His research interests include computational electromagnetics, electromagnetic compatibility, and wireless power transfer.

Dr. Pichon is an Associate Editor for the European Physical Journal Applied Physics (EPJ AP) and Journal of Electromagnetic Waves and Applications.

MOHAMED BENSETTI received the masters degree (DEA), the Ph.D. degree in electrical engineering, and the Habilitation Diriger des Recherches degree from the University of Paris-Sud, Orsay, France, in 2001 and 2004, and 2014, respectively

From 2005 to 2007, he was a Researcher with Ecole Supérieure dElectricité (SUPELEC), Gif sur Yvette, France. In 2007, he joined Ecole Supérieure dIngénieur en Génie Electrique (ESIG-ELEC), Rouen, France, where he was a Lecturer and a Researcher with the Research Institute for Electronic Embedded Systems (IRSEEM). In January 2013, he joined the Energy Department, SUPELEC, Gif-sur-Yvette, France. He is currently a Professor with Centrale-Supelec, Gif-sur-Yvette. He is currently with Group of electrical engineering, Paris (GeePs). His current research interests include electromagnetic modeling, electromagnetic compatibility (EMC), power electronics, and wirless power transmission, including modeling, simulation, and instrumentation.

FABRIZIO DUGHIERO received the M.S. degree in electrical engineering from the University of Padova, Padua, Italy, in 1988.

He is currently a Full Professor of Electromagnetic Processing of Materials (EPM) with Universitá degli Studi di Padova, Padua, and the Chief Scientist with the Laboratory of Electroheat, Universitá degli Studi di Padova. He has been the Founder of a spin-off company (InovaLab) and Unismart Padua Enterprise Ltd., Padua, a new in-house company aimed to develop Technology and Knowledge Transfer of Universitá degli Studi di Padova. He is currently the Director of the Department of Industrial Engineering, Universitá degli Studi di Padova. His current research interests, documented by more than 180 scientific publications, include theoretical aspects and applications of EPM and electroheat technologies.